3-18-2009

Modeling Gravitational Recoil from Precessing Highly-Spinning Unequal-Mass Black-Hole Binaries

Carlos O. Lousto
Rochester Institute of Technology

Yosef Zlochower
Rochester Institute of Technology

Recommended Citation
C. Lousto and Y. Zlochower, Phys. Rev. D 79, 064018 (2009). https://doi.org/10.1103/PhysRevD.79.064018

Modeling gravitational recoil from precessing highly-spinning unequal-mass black-hole binaries

Carlos O. Lousto and Yosef Zlochower

Center for Computational Relativity and Gravitation,
School of Mathematical Sciences, Rochester Institute of Technology,
78 Lomb Memorial Drive, Rochester, New York 14623

(Dated: January 1, 2009)

We measure the gravitational recoil for unequal-mass-black-hole-binary mergers, with the larger BH having spin $a/m^H = 0.8$, and the smaller BH non-spinning. We choose our configurations such that, initially, the spins lie on the orbital plane. The spin and orbital plane precess significantly, and we find that the out-of plane recoil (i.e. the recoil perpendicular to the orbital plane around merger) varies as $\eta^2/(1+q)$, in agreement with our previous prediction, based on the post-Newtonian scaling.

PACS numbers: 04.25.Dm, 04.25.Nx, 04.30.Db, 04.70.Bw

I. INTRODUCTION

The recent observational discovery of a possible recoiling supermassive black hole at a speed of 2650 $\mathrm{km\,s^{-1}}$ with respect to its host galaxy [1] represent the first observational evidence in support of the predictions of General Relativity in the strong-field, highly-dynamical, and highly-nonlinear regime. This recoil, if it in fact resulted from a black-hole merger, would confirm the theoretical prediction of Campanelli et al. [2] that black-hole mergers can lead to very large recoils. This original prediction, and the subsequent calculation [3] that indicated that such recoils can be as large as 4000 $\mathrm{km\,s^{-1}}$, has been a key trigger for the recent theoretical efforts to determine EM signatures of large recoils and the astronomical searches for these signatures [1, 4, 5, 6, 7, 8].

Thanks to recent breakthroughs in the full non-linear numerical evolution of black-hole-binary spacetimes [9, 10, 11], it is now possible to accurately simulate the merger process and examine its effects in this highly nonlinear regime [12, 13, 14, 15, 16, 17, 18, 19, 20, 21, 22, 23, 24, 25, 26]. Black-hole binaries will radiate between 2% and 8% of their total mass and up to 40% of their angular momenta, depending on the magnitude and direction of the spin components, during the merger [14, 15, 16]. In addition, the radiation of net linear momentum by a black-hole binary leads to the recoil of the final remnant hole [2, 3, 7, 27, 28, 29, 30, 31, 32, 33, 34, 35, 36, 37, 38, 39, 40, 41, 42, 43, 44, 45, 46, 47], which can have astrophysically important effects [2, 7, 48, 49, 50, 51].

In [2] we introduced the following heuristic model for the gravitational recoil of a merging binary.

$$\vec{V}_{\rm recoil}(q,\vec{\alpha}_i) = v_m\,\hat{e}_1 + v_\perp(\cos(\xi)\,\hat{e}_1 + \sin(\xi)\,\hat{e}_2) + v_\parallel\,\hat{e}_z, \tag{1}$$

where

$$v_m = A\frac{\eta^2(1-q)}{(1+q)}\,(1+B\,\eta)\,, \tag{2a}$$

$$v_\perp = H\frac{\eta^2}{(1+q)}\left(\alpha_2^\parallel - q\alpha_1^\parallel\right), \tag{2b}$$

$$v_\parallel = K\cos(\Theta-\Theta_0)\frac{\eta^2}{(1+q)}\left|\vec{\alpha}_2^\perp - q\vec{\alpha}_1^\perp\right|, \tag{2c}$$

$A = 1.2\times10^4$ $\mathrm{km\,s^{-1}}$ [31], $B = -0.93$ [31], $H = (6.9\pm0.5)\times10^3$ $\mathrm{km\,s^{-1}}$, $\vec{\alpha}_i = \vec{S}_i/m_i^2$, $\vec{S}_i$ and m_i are the spin and mass of hole i, $q = m_1/m_2$ is the mass ratio of the smaller to larger mass hole, $\eta = q/(1+q)^2$ is the symmetric mass ratio, the index $\perp$ and $\parallel$ refer to perpendicular and parallel to the orbital angular momentum respectively at the effective moment of the maximum generation of the recoil (around merger time), $\hat{e}_1, \hat{e}_2$ are orthogonal unit vectors in the orbital plane, and ξ measures the angle between the "unequal mass" and "spin" contributions to the recoil velocity in the orbital plane. The angle Θ was defined as the angle between the in-plane component of $\vec{\Delta} \equiv (m_1+m_2)(\vec{S}_2/m_2 - \vec{S}_1/m_1)$ and the infall direction at merger. The form of Eq. (2a) was proposed in [31, 52], while the form of Eqs. (2b) and (2c) was proposed in [2] based on the post-Newtonian expressions in [53]. In Ref [3] we determined that $K = (6.0\pm0.1)\times10^4$ $\mathrm{km\,s^{-1}}$, and made the first prediction that the maximum possible recoil is ~ 4000 $\mathrm{km\,s^{-1}}$ for equal-mass binaries with anti-parallel spins in the orbital plane (in Ref. [47], we performed simulations with a measured recoil of 3250 $\mathrm{km\,s^{-1}}$). Although ξ may in general depend strongly on the configuration, the results of [37] and post-Newtonian [53] calculations show that ξ is 90° for headon collisions, and the results presented in Ref. [54] indicate that $\xi \sim 145°$ for a wide range of quasi-circular configurations. A simplified version of Eq. (1) that models the magnitude of $V_{\rm recoil}$ was independently proposed in [39], and a simplified form of Eq. (2b) for the equal-mass aligned spin case was proposed in [36]. A more general formula, using only symmetry arguments and fits to numerical data, was recently proposed in [55, 56].

Our heuristic formula (1) describing the recoil velocity of a black-hole binary remnant as a function of the parameters of the individual holes has been theoretically verified in several ways. In [3] the $\cos\Theta$ dependence was established and was confirmed in [43] for binaries with different initial separations. In Ref. [42] the decomposi-

tion into spin components perpendicular and parallel to the orbital plane was verified, and in [46] it was found that the quadratic-in-spin corrections to the in-plane recoil velocity are less than 20 $\mathrm{km\,s^{-1}}$. Recently, Baker et al. [57] measured the recoil for unequal-mass, spinning binaries, with spins lying in the initial orbital plane, and concluded that the leading order dependence of the out-of-plane kick was $\mathcal{O}(\eta^3)$, rather than the $\mathcal{O}(\eta^2)$ that we predicted. In this paper we examine this dependence in detail.

As pointed out in [57] the consequences of an $\mathcal{O}(\eta^3)$ dependence of the recoil, rather than an $\mathcal{O}(\eta^2)$ dependence, are significant for both the retention of intermediate mass black holes (IMBH) in globular clusters and supermassive black holes in galaxies. It is thus important that we understand how the recoil depends on mass ratio.

In their paper, Baker et al. [57] analyzed configurations that required fitting two angle parameters (for a given value of q) before the maximum recoil could be obtained. Their configuration also produced very small recoil velocities for smaller values of q. In order to help clearly display the dependence, we choose configurations that only require fitting one angle parameter in Eq. (2c), and have a substantial recoil even for our smallest mass ratios. In addition, the Baker et al. [57] runs were constructed such that the spin of the larger black hole is proportional to the mass ratio squared times the spin of the smaller BH, i.e. $\alpha_2 = q^2\alpha_1$, where $q = m_1/m_2 < 1$, and $\alpha_1 < 1$ is the spin of the smaller black hole. In the small mass ratio limit, this leads to a small, very highly rotating hole (for any spin-induced recoil to be observable) orbiting a large, essentially nonrotating, BH. This configuration does not match the expected astrophysical scenario since large BHs are expected to have high spins. Our choice of configuration more closely matches the astrophysical scenario when $q \to 0$ because in that limit the recoil becomes independent of the spin of the smaller BH, as is apparent in the factor of $\alpha_2 - q\alpha_1$ in Eq. (2c).

The paper is organized as follows, in Sec. II we review the numerical techniques used for the evolution of the black-hole binaries and the analysis of the physical quantities extracted at their horizons, in Sec. III we present results and analysis, and in Sec. IV we present our conclusions.

II. TECHNIQUES

To compute initial data, we use the puncture approach [58] along with the TwoPunctures [59] thorn. In this approach the 3-metric on the initial slice has the form $\gamma_{ab} = (\psi_{BL} + u)^4\delta_{ab}$, where ψ_{BL} is the Brill-Lindquist conformal factor, δ_{ab} is the Euclidean metric, and u is (at least) C^2 on the punctures. The Brill-Lindquist conformal factor is given by $\psi_{BL} = 1 + \sum_{i=1}^{n} m_i^p/(2|\vec{r}-\vec{r}_i|)$, where n is the total number of 'punctures', m_i^p is the mass parameter of puncture i (m_i^p is *not* the horizon mass associated with puncture i), and $\vec{r}_i$ is the coordinate location of puncture i. We evolve these black-hole-binary data-sets using the LazEv [60] implementation of the moving puncture approach [10, 11]. In our version of the moving puncture approach we replace the BSSN [61, 62, 63] conformal exponent ϕ, which has logarithmic singularities at the punctures, with the initially C^4 field $\chi = \exp(-4\phi)$. This new variable, along with the other BSSN variables, will remain finite provided that one uses a suitable choice for the gauge. An alternative approach uses standard finite differencing of ϕ [11]. Recently Marronetti et al. [64] proposed the use of $W = \sqrt{\chi}$ as an evolution variable. For the runs presented here we use centered, eighth-order finite differencing in space [65] and an RK4 time integrator (note that we do not upwind the advection terms).

We use the CACTUS framework [66] with the CARPET [67] mesh refinement driver to provide a 'moving boxes' style mesh refinement. In this approach refined grids of fixed size are arranged about the coordinate centers of both holes. The CARPET code then moves these fine grids about the computational domain by following the trajectories of the two black holes.

We obtain accurate, convergent waveforms and horizon parameters by evolving this system in conjunction with a modified 1+log lapse and a modified Gamma-driver shift condition [10, 68], and an initial lapse $\alpha(t=0) = 2/(1+\psi_{BL}^4)$. The lapse and shift are evolved with

$$(\partial_t - \beta^i\partial_i)\alpha = -2\alpha K \tag{3a}$$

$$\partial_t\beta^a = B^a \tag{3b}$$

$$\partial_t B^a = 3/4\partial_t\tilde{\Gamma}^a - \sigma B^a. \tag{3c}$$

Note that we denote the Gamma-driver parameter by σ rather than the more typical η to avoid confusion with the symmetric mass ratio parameter. These gauge conditions require careful treatment of χ, the inverse of the three-metric conformal factor, near the puncture in order for the system to remain stable [10, 12, 20]. In our tests, W showed better behavior at very early times ($t < 10M$) (i.e. did not require any special treatment near the punctures), but led to evolutions with lower effective resolution when compared to χ. Interestingly, a mixed evolution system that evolved W for $t < 10M$ and χ for $t > 10M$ showed inaccuracies similar to the pure W system. At higher resolution W and χ agreed with good accuracy. In Ref. [69] it was shown that this choice of gauge leads to a strongly hyperbolic evolution system provided that the shift does not become too large.

We use AHFinderDirect [70] to locate apparent horizons. We measure the magnitude of the horizon spin using the Isolated Horizon algorithm detailed in [71]. This algorithm is based on finding an approximate rotational Killing vector (i.e. an approximate rotational symmetry) on the horizon, and given this approximate Killing vector φ^a, the spin magnitude is

$$S_{[\varphi]} = \frac{1}{8\pi}\oint_{AH}(\varphi^a R^b K_{ab})d^2V \tag{4}$$

where K_{ab} is the extrinsic curvature of the 3D-slice, d^2V is the natural volume element intrinsic to the horizon, and R^a is the outward pointing unit vector normal to the horizon on the 3D-slice. We measure the direction of the spin by finding the coordinate line joining the poles of this Killing vector field using the technique introduced in [16]. Our algorithm for finding the poles of the Killing vector field has an accuracy of $\sim 2^\circ$ (see [16] for details). The mass of the horizon is given by the Christodoulou formula

$$m^H = \sqrt{m_{\rm irr}^2 + S^2/(4m_{\rm irr}^2)}, \tag{5}$$

where $m_{\rm irr}$ is the irreducible mass.

We also use an alternative quasi-local measurement of the spin and linear momentum of the individual black holes in the binary that is based on the coordinate rotation and translation vectors [45]. In this approach the spin components of the horizon are given by

$$S_{[i]} = \frac{1}{8\pi} \oint_{AH} \phi^a_{[i]} R^b K_{ab} d^2V, \tag{6}$$

where $\phi^i_{[\ell]} = \delta_{\ell j}\delta_{mk} r^m \epsilon^{ijk}$, and $r^m = x^m - x_0^m$ is the coordinate displacement from the centroid of the hole, while the linear momentum is given by

$$P_{[i]} = \frac{1}{8\pi} \oint_{AH} \xi^a_{[i]} R^b (K_{ab} - K\gamma_{ab}) d^2V, \tag{7}$$

where $\xi^i_{[\ell]} = \delta^i_\ell$.

We measure radiated energy, linear momentum, and angular momentum, in terms of ψ_4, using the formulae provided in Refs. [72, 73]. However, rather than using the full ψ_4 we decompose it into ℓ and m modes and solve for the radiated linear momentum, dropping terms with $\ell \geq 5$ (only the $\ell = 2$ and $\ell = 3$ modes make significant contributions to the recoil). The formulae in Refs. [72, 73] are valid at $r = \infty$. We obtain highly accurate values for these quantities by solving for them on spheres of finite radius (typically $r/M = 50, 60, \cdots, 100$), fitting the results to a polynomial dependence in $l = 1/r$, and extrapolating to $l = 0$. We perform fits based on a linear and quadratic dependence on l, and take the final values to be the quadratic extrapolation with the differences being the extrapolation error.

A. Initial Data

We evolve quasi-circular configurations with a more massive spinning black hole, with specific spin $a/m^H = 0.8$ pointing in the initial orbital plane, and a non-spinning smaller BH. The orbital parameters where chosen using 3PN parameters for quasi-circular orbits with orbital period $M\omega = 0.05$, which provides the puncture locations and momenta. We normalize the puncture mass parameters so that the total ADM mass is $1M$ and the mass ratio is the specified one. We then modify the configurations by rotating the initial spin direction (which has a small effect on the total ADM mass). We denote these configurations by QXXXTHYYY, where XXX denotes the mass ratio (XXX=100 for $q = 1$, XXX=66 for $q = 2/3$, XXX=50 for $q = 1/2$, XXX=40 for $q = 1/2.5$, XXX=33 for $q = 1/3$, XXX=25 for $q = 1/4$, XXX=17 for $q = 1/6$, and XXX=13 for $q = 1/8$) and YYY gives the angle (in degrees) between the initial spin direction and the y-axis. The initial data parameters are summarized in Table I. These configuration have several advantages when modeling the out-of-plane kick as a function of mass ratio. First, one need only fit to two parameters (one angle and one amplitude) to determine the maximum recoil for a given mass ratio; improving the statistical reliability of the estimated maximum recoil. Second, the maximum recoil velocity is quite large, even for $q = 1/6$, ensuring that errors in measuring the maximum recoil velocity are not a significant fraction of the recoil itself. In addition the functional form used in our non-linear fits, $A\cos(\vartheta - B)$, yields a more robust measurement of A when compared to fits of $C\cos(\vartheta_1 - D) + E\cos(\vartheta_2 - F)$ (as used in Baker et al.) for small sample sizes (i.e. the functional form used here is more amenable to an accurate fit when the sample size is small). (See Fig. 5)

B. Determining the Orbital Plane

These configuration show significant orbital precession, as demonstrated in Fig. 1, that presents a significant challenge when modeling the recoil. Our empirical formula (1) decomposes the recoil in terms of velocities parallel and perpendicular to the angular momentum. Thus we need an accurate determination of the orbital plane near merger (where most of the recoil is generated [43, 54]). We determine an approximate plane by choosing points along the plunge trajectory near where $|\dot{r}|$ and $|\ddot{r}|$ have extrema. We then find a rotation, such that the late-time approximate orbital plane is rotated onto the xy-plane. In order to model the out-of-plane recoil, we need to measure it as a function of the orientation of the spin vector during merger. We do this by fixing the remaining freedom in the transformation such that the transformed trajectories (for a given sequence of configurations) coincide (approximately) near merger. We then measure the spin direction at some fixed fiducial point along the merger trajectory (in practice, at the point r_0 discussed below) and fit the out-of-plane kick to the form $V = A\cos(\vartheta - B)$, where ϑ is the angle between the in-plane component of the spin at this fiducial point

TABLE I: Initial data parameters for the quasi-circular configurations with a non-spinning smaller mass black hole (labeled 1), and a larger spinning black hole (labeled 2). The punctures are located at $\vec{r}_1 = (x_1, 0, 0)$ and $\vec{r}_2 = (x_2, 0, 0)$, with momenta $P = \pm(0, P, 0)$, spins $\vec{S}_2 = (S_x, S_y, 0)$, mass parameters m^p, horizon (Christodoulou) masses m^H, and total ADM mass $M_{\rm ADM}$. The configuration are denoted by QXXXTHYYY where XXX gives the mass ratio (0.17, 0.25, 0.40, 0.33, 0.50, 0.66, 1.00) and YYY gives the angle in degrees between the initial spin direction and the y-axis. In all cases the initial orbital period is $M\omega = 0.05$.

Config	x_1/M	x_2/M	P/M	m_1^p	m_2^p	S_x/M^2	S_y/M^2	m_1^H	m_2^H	$M_{\rm ADM}/M$	a/m^H
Q13TH000	5.70322	-0.69841	0.054063	0.10174	0.55179	0.00000	0.63913	0.11114	0.88910	1.00000	0.8086
Q13TH090	5.70322	-0.69841	0.054063	0.10174	0.55179	-0.63913	0.00000	******	0.88909	1.00005	0.8086
Q13TH130	5.70322	-0.69841	0.054063	0.10174	0.55179	-0.48961	-0.41083	******	0.88909	1.00003	0.8086
Q13TH210	5.70322	-0.69841	0.054063	0.10174	0.55179	0.31957	-0.55351	******	0.88909	1.00001	0.8086
Q13TH315	5.70322	-0.69841	0.054063	0.10174	0.55179	0.45194	0.45194	******	0.88909	1.00003	0.8086
Q17TH000	5.52270	-0.90366	0.066761	0.13153	0.53157	0.00000	0.59594	0.14310	0.85859	1.00000	0.8084
Q17TH090	5.52270	-0.90366	0.066761	0.13153	0.53157	-0.59594	0.00000	******	0.85858	1.00004	0.8084
Q17TH130	5.52270	-0.90366	0.066761	0.13153	0.53157	-0.45651	-0.38306	******	0.85858	1.00002	0.8084
Q17TH210	5.52270	-0.90366	0.066761	0.13153	0.53157	0.29797	-0.51610	******	0.85858	1.00001	0.8084
Q17TH315	5.52270	-0.90366	0.066761	0.13153	0.53157	0.42139	0.42139	******	0.85858	1.00002	0.8084
Q25TH000	5.18788	-1.27783	0.086696	0.18588	0.49511	0.00000	0.52144	0.20081	0.80326	1.00000	0.8082
Q25TH090	5.18788	-1.27783	0.086696	0.18588	0.49511	-0.52144	0.00000	0.20094	0.80324	1.00000	0.8082
Q25TH130	5.18788	-1.27783	0.086696	0.18588	0.49511	-0.39945	-0.33518	0.20080	0.80325	1.00000	0.8082
Q25TH210	5.18788	-1.27783	0.086696	0.18588	0.49511	0.26072	-0.45158	0.20081	0.80325	1.00000	0.8082
Q25TH315	5.18788	-1.27783	0.086696	0.18588	0.49511	0.36871	0.36871	0.20081	0.80325	1.00000	0.8032
Q33TH000	4.88556	-1.60904	0.101152	0.23415	0.46316	0.00000	0.45982	0.25147	0.75443	1.00000	0.8079
Q33TH090	4.88556	-1.60904	0.101152	0.23415	0.46316	-0.45982	0.00000	0.25144	0.75437	0.99994	0.8080
Q33TH130	4.88556	-1.60904	0.101152	0.23415	0.46316	-0.35224	-0.29557	0.25145	0.75440	0.99996	0.8080
Q33TH210	4.88556	-1.60904	0.101152	0.23415	0.46316	0.22991	-0.39822	0.25162	0.75443	0.99998	0.8079
Q33TH315	4.88556	-1.60904	0.101152	0.23415	0.46316	0.32514	0.32514	0.25145	0.75441	0.99997	0.8080
Q40TH000	4.66490	-1.84716	0.109810	0.26900	0.44033	0.00000	0.41792	0.28772	0.71930	1.00000	0.8077
Q40TH090	4.66490	-1.84716	0.109810	0.26900	0.44033	-0.41792	0.00000	0.28771	0.71927	0.99990	0.8079
Q40TH130	4.66490	-1.84716	0.109810	0.26900	0.44033	-0.32014	-0.26863	0.28771	0.71927	0.99994	0.8078
Q40TH210	4.66490	-1.84716	0.109810	0.26900	0.44033	0.20896	-0.36193	0.28771	0.71929	0.99997	0.8077
Q40TH315	4.66490	-1.84716	0.109810	0.26900	0.44033	0.29551	0.29551	0.28771	0.71929	0.99995	0.8078
Q50TH000	4.36532	-2.16588	0.119233	0.31591	0.40994	0.00000	0.36487	0.33611	0.67223	1.00001	0.8074
Q50TH090	4.36532	-2.16588	0.119233	0.31591	0.40994	-0.36487	0.00000	0.33609	0.67217	0.99984	0.8076
Q50TH130	4.36532	-2.16588	0.119233	0.31591	0.40994	-0.27950	-0.23453	0.33611	0.67220	0.99991	0.8076
Q50TH210	4.36532	-2.16588	0.119233	0.31591	0.40994	0.18243	-0.31598	0.33611	0.67222	0.99997	0.8074
Q50TH315	4.36532	-2.16588	0.119233	0.31591	0.40994	0.25800	0.25800	0.33613	0.67221	0.99993	0.8075
Q66TH000	3.93712	-2.61286	0.128421	0.38234	0.36743	0.00000	0.29620	0.40390	0.60587	1.00000	0.8069
Q66TH090	3.93712	-2.61286	0.128421	0.38234	0.36743	-0.29620	0.00000	0.40389	0.60579	0.99975	0.8072
Q66TH130	3.93712	-2.61286	0.128421	0.38234	0.36743	-0.22690	-0.19039	0.40388	0.60582	0.99985	0.8071
Q66TH210	3.93712	-2.61286	0.128421	0.38234	0.36743	0.14810	-0.25651	0.40389	0.60585	0.99994	0.8070
Q66TH315	3.93712	-2.61286	0.128421	0.38234	0.36743	0.20944	0.20944	0.40389	0.60583	0.99988	0.8071
Q100TH000	3.28027	-3.28027	0.133568	0.48338	0.30398	0.00000	0.20595	0.50543	0.50547	1.00001	0.8061
Q100TH090	3.28027	-3.28027	0.133568	0.48338	0.30398	-0.20595	0.00000	0.50541	0.50537	0.99965	0.8065
Q100TH130	3.28027	-3.28027	0.133568	0.48338	0.30398	-0.15777	-0.13238	0.50542	0.50541	0.99980	0.8063
Q100TH210	3.28027	-3.28027	0.133568	0.48338	0.30398	0.10297	-0.17836	0.50543	0.50544	0.99992	0.8062
Q100TH315	3.28027	-3.28027	0.133568	0.48338	0.30398	0.14563	0.14563	0.50542	0.50542	0.99983	0.8063

for a given configuration with the in-plane spin for the corresponding QXXXTH000 configuration.

We determine the orbital plane during merger in the following way. We plot $r = |\vec{r}_1 - \vec{r}_2|$ as a function of time and determine the location of the maximum of $|\dot{r}|$. We then choose two points on either side of the maximum with similar values of $|\dot{r}|$ and a third point close to the maximum. We denote these three points of the trajectory with $\vec{r}_+$, $\vec{r}_0$, and $\vec{r}_-$. We then choose a rotation such that the vector $\vec{r}_a = \vec{r}_+ - \vec{r}_0$ lies on the new

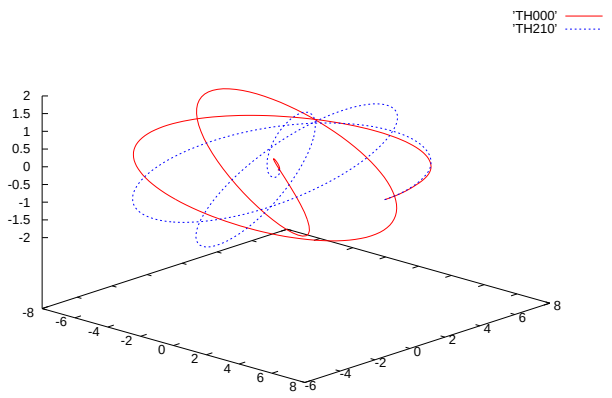

FIG. 1: The trajectory $\vec{r}_1 - \vec{r}_2$ for the Q25TH000 and Q25TH210 configurations. Note the significant precession and the lack of alignment between the late-time orbital planes.

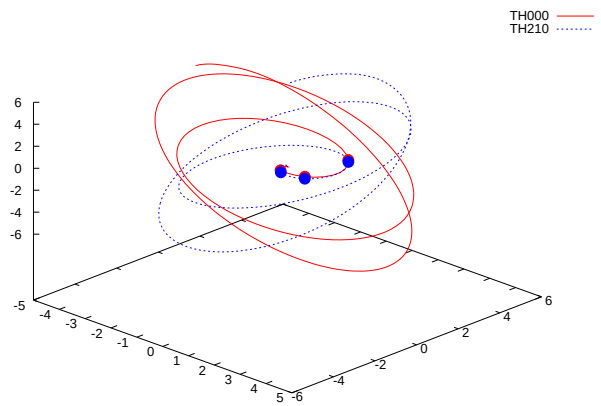

FIG. 2: The trajectory $\vec{r}_1 - \vec{r}_2$ for the Q25TH000 and Q25TH210 configurations after rotating the system. Note the good agreement in the late time trajectories and that these trajectories now lie on the xy plane. The solid points are the locations of $\vec{r}_+$, $\vec{r}_0$, and $\vec{r}_-$. Note that these points agree for both curves.

y-axis and that the normal to the plane determined by $\vec{r}_a$ and $\vec{r}_b = \vec{r}_- - \vec{r}_0$ lies along the new z-axis. With these choices we uniquely determine a rotational transformation from the coordinates used by the code to coordinates where the plunging orbital plane coincides with the xy plane. This transformation also rotates the trajectories in the appropriate way such that trajectories with similar late-time dynamics will overlap during merger (this is a generalization of the procedure given in Ref. [47, 54]).

In Fig. 1 we show the orbital trajectory difference $\vec{r}_1 - \vec{r}_2$ for the Q25TH000 and Q25TH210 configurations. Note the significant precession and that the orbital planes near merger do not coincide. Fig. 2 shows that, after rotating the plane, as described above, the merger trajectories coincide.

In Figs. 3 and 4 we show the xy projections of the trajectories for the Q25THYYY configurations before and after rotating the merger orbital plane. Note that prior to this transformation, there is no rotation in the xy plane that will make the late-time trajectories overlap and the reasonable overlap of the late-time trajectories for the transformed case.

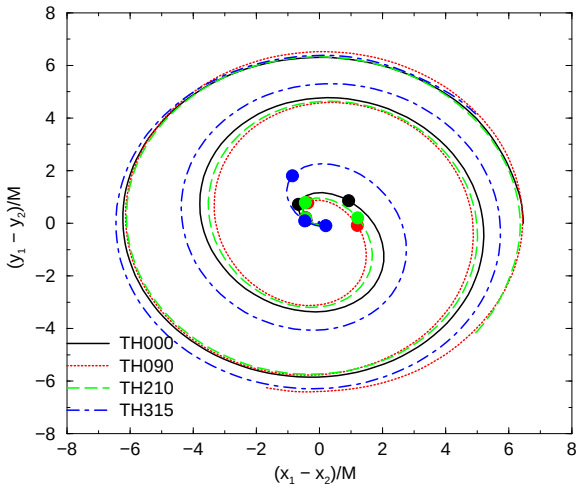

FIG. 3: The xy projection for the untransformed trajectory $\vec{r}_1 - \vec{r}_2$ for the Q25THYYY configurations. The trajectories have been rotated (in the xy plane). Note that there are no rotations in the xy plane that will make the late-time trajectories overlap. The filled circles are the locations of $\vec{r}_+$, $\vec{r}_0$, and $\vec{r}_-$.

III. RESULTS

We used the following grid configurations for the runs. For the $q = 1/2$, $q = 1/2.5$, and $q = 1/3$ runs we placed the outer boundaries at $1664M$ with a coarsest resolution of $h = 25.6M$, we used 12 levels of refinement around the smaller BH, with finest resolution of $h = M/80$, and 11 levels of refinement around the larger BH. For the $q = 1/4$ runs we added an additional level of refinement around the smaller BH, for $q = 1/6$ and $q = 1/8$ we added two additional levels (for a total of 14), and for the $q = 2/3$ runs we added an additional level of refinement about the larger BH. For the $q = 1$ runs we used 11 levels of refinement around the non-spinning hole and 12 levels of refinement around the spinning hole. In the $q = 1/4$ case, we found that using eighth-order accuracy was critical, as incorrect dynamics (outspiral rather than inspiral when evolving with χ, and plunges rather than inspirals when evolving with W) resulted when using fourth order methods. The dynamics obtained from the W and χ systems agreed when using eighth-order methods. In all cases we used $\sigma = 3$ in the Gamma-driver shift condition. In addition we ran all $q = 1/4$ configuration with a higher resolution (by a factor of 1.2) for all levels (See

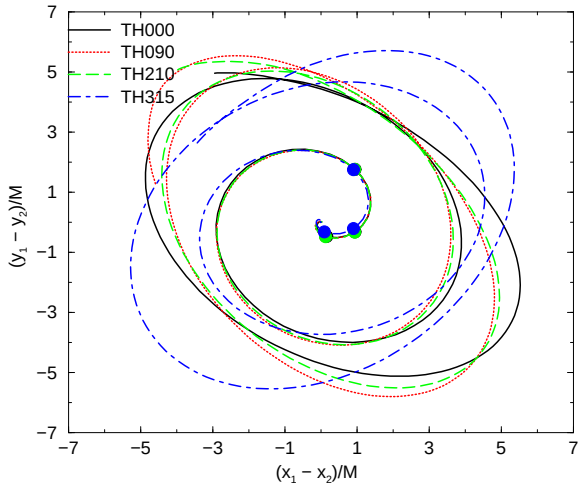

FIG. 4: The xy projection for the transformed trajectory $\vec{r}_1 - \vec{r}_2$ for the Q25THYYY configurations. No additional rotations have been applied. Note the good agreement in the late time trajectories. The filled circles are the locations of $\vec{r}_+$, $\vec{r}_0$, and $\vec{r}_-$.

In order to measure the dependence of our recoil calculations on the choice of r_+, r_0, r_- (the three points in the trajectory that define the late-time orbital plane) we make two choices for these quantities a fiducial choice $(r_+, r_0, r_-)/M = (2.0, 1.0, 0.5)$ and a second choice $(r_+, r_0, r_-)/M = 2.2, 1.2, 0.7)$ based on the point in the orbital trajectory when $|\dot{r}(r)|$ is a maximum. For our runs we found that the maximum in $|\dot{r}(t)|$ occurs at $r = (1.2 \pm 0.1)$. We also use an alternative approach, discussed in Sec. III C, where we choose (r_+, r_0, r_-) to be the extrema of $\dot{r}(t)$ and $\ddot{r}(t)$ during the plunge phase. In this latter approach, the values of (r_+, r_0, r_-) vary with each configuration and generally produce poorer results than for the fixed choice of (r_+, r_0, r_-). In Table III we show how these two choices affect the calculation of $v_\parallel$ and $v_\perp$, the spin component in and out of the plane, and the angle between the in-plane spins with the corresponding spin for the TH000 configurations (ϑ). Note that we report the magnitude of the in-plane (i.e. $v_\perp$) recoil and spin $a_\perp$, because modifying (r_+, r_0, r_-) introduces additional rotations within the orbital plane; making a direct comparison of x and y components meaningless. Note that there is scatter in both the in-plane and out-plane components of the spin. The scatter in the out-of-plane component appears to be relatively significant due to its small average value. The source of this scatter may simply be due to errors in estimating the true direction of the orbital plane (since the spin in the plane is large). We take the average value of the in-plane spin when fitting to Eq. (1) below.

Our empirical formula (1) predicts that $v_\parallel$ will scale as $\cos(\vartheta - \vartheta_0)$. For each set of configurations with a given mass ratio, we perform a non-linear least squares fit of $v_\parallel$ to the form

$$v_\parallel = A\cos(\vartheta - B) \tag{8}$$

and solve for A and B. The results of these fits are summarized in Table IV. In Fig. 5 we plot the individual data points for each mass ratio and the best fit function. Note that the effect of refining the grid is to slightly increase the magnitude of the out-of-plane recoil.

With the above results we can now fit the maximum out-of-plane recoil ($v_\parallel$) versus q. Our empirical formula (1) predicts that this maximum will have the form $v_\parallel = K\eta^2/(1+q)(\alpha_1 - q\alpha_2)$, where $\eta = q/(1+q)^2$. For all of our configurations $\alpha_2 \approx 0$, and hence $v_\parallel = \alpha_1 K\eta^2/(1+q)$. Interestingly, this form has a maximum

Sec. III A).

In Table II we give the radiated energy and angular momenta for all configurations, as well as the untransformed recoil velocities.

TABLE II: The radiated energy and angular momentum, as well as the recoil velocities for each configuration. Note that some of the error estimates, which are based on the differences between a linear and quadratic extrapolation in $l = 1/r$, are very small. This indicates that the differences between the extrapolation can underestimate the true error. All quantities are given in the coordinate system used by the code (i.e. the untransformed system). The Q25THXXX quantities given on the bottom of the table are for the higher resolution runs. See Sec. III A for an explanation of the differences in the radiated quantities.

Config	$100E/M$	$100J_x/M^2$	$100J_y/M^2$	$100J_z/M^2$	V_x	V_y	V_z
Q13TH000	0.623 ± 0.018	2.383 ± 0.031	1.987 ± 0.050	2.002 ± 0.035	66.5 ± 2.3	26.9 ± 5.0	101.0 ± 6.8
Q13TH090	0.6444 ± 0.005	-2.182 ± 0.008	2.533 ± 0.017	2.142 ± 0.184	-14.2 ± 6.5	70.7 ± 3.3	92.7 ± 6.3
Q13TH130	0.671 ± 0.013	-3.438 ± 0.034	0.509 ± 0.008	2.112 ± 0.012	-393.0 ± 11.9	-167.4 ± 15.3	43.2 ± 0.1
Q13TH210	0.637 ± 0.007	-1.072 ± 0.031	-2.980 ± 0.038	2.199 ± 0.140	38.1 ± 3.9	86.3 ± 2.8	-97.1 ± 7.5
Q13TH315	0.689 ± 0.011	3.484 ± 0.041	-0.161 ± 0.009	2.162 ± 0.049	-382.0 ± 12.3	-216.2 ± 17.3	-27.2 ± 0.2
Q17TH000	1.032 ± 0.0343	3.644 ± 0.027	3.990 ± 0.094	3.70 ± 0.094	-99.5 ± 10.8	-624.5 ± 27.6	-137.9 ± 6.8
Q17TH090	0.980 ± 0.005	-4.133 ± 0.014	3.903 ± 0.078	3.66 ± 0.246	323.1 ± 5.2	-105.5 ± 1.8	-146.1 ± 10.0
Q17TH130	1.049 ± 0.027	-5.592 ± 0.059	0.004 ± 0.014	3.484 ± 0.045	371.8 ± 10.4	343.2 ± 16.4	-42.3 ± 0.3
Q17TH210	1.027 ± 0.032	-1.162 ± 0.011	-5.351 ± 0.100	3.70 ± 0.077	228.6 ± 21.5	-579.2 ± 14.8	140.8 ± 5.4
Q17TH315	1.032 ± 0.012	5.401 ± 0.044	0.352 ± 0.035	3.687 ± 0.222	175.0 ± 8.3	270.0 ± 10.6	-30.3 ± 3.5
Q25TH000	1.621 ± 0.020	4.543 ± 0.135	5.521 ± 0.044	7.571 ± 0.115	145.1 ± 15.6	855.3 ± 21.9	535.3 ± 9.9
Q25TH090	1.642 ± 0.016	-5.895 ± 0.076	4.412 ± 0.039	7.868 ± 0.233	-869.9 ± 19.8	80.5 ± 14.2	446.3 ± 7.4
Q25TH130	1.530 ± 0.012	-6.879 ± 0.040	-0.096 ± 0.005	7.400 ± 0.209	-64.7 ± 9.1	-141.3 ± 3.5	-131.7 ± 2.2
Q25TH210	1.638 ± 0.018	-1.045 ± 0.106	-7.132 ± 0.021	7.776 ± 0.062	-335.9 ± 27.8	819.1 ± 17.2	-487.8 ± 8.5
Q25TH315	1.512 ± 0.014	6.774 ± 0.063	0.583 ± 0.030	7.375 ± 0.188	73.4 ± 7.1	-45.9 ± 0.4	223.4 ± 3.9
Q33TH000	2.216 ± 0.023	4.731 ± 0.073	7.171 ± 0.087	11.516 ± 0.098	47.5 ± 19.1	983.3 ± 19.6	827.3 ± 8.8
Q33TH090	2.184 ± 0.018	-7.569 ± 0.026	4.653 ± 0.040	11.548 ± 0.082	-829.1 ± 21.2	-40.4 ± 15.5	576.6 ± 8.0
Q33TH130	2.050 ± 0.016	-8.485 ± 0.017	-0.840 ± 0.053	11.108 ± 0.089	171.0 ± 4.8	8.7 ± 0.2	-374.3 ± 0.3
Q33TH210	2.200 ± 0.020	-0.433 ± 0.081	-8.597 ± 0.062	11.515 ± 0.032	-453.0 ± 26.2	793.0 ± 12.0	-697.3 ± 6.7
Q33TH315	2.054 ± 0.017	8.335 ± 0.022	1.495 ± 0.010	11.072 ± 0.002	306.9 ± 5.6	155.7 ± 5.4	520.5 ± 0.7
Q40TH000	2.613 ± 0.021	4.604 ± 0.114	8.337 ± 0.024	14.791 ± 0.074	19.6 ± 19.4	985.0 ± 15.0	1132.5 ± 4.8
Q40TH090	2.607 ± 0.017	-8.761 ± 0.001	4.729 ± 0.133	14.790 ± 0.147	-929.8 ± 18.2	-83.4 ± 16.3	939.3 ± 6.4
Q40TH130	2.452 ± 0.012	-9.332 ± 0.033	-1.734 ± 0.082	14.123 ± 0.130	-12.3 ± 1.7	-168.0 ± 5.5	-137.0 ± 3.6
Q40TH210	2.621 ± 0.018	0.157 ± 0.047	-9.604 ± 0.013	14.815 ± 0.072	-520.1 ± 24.9	845.9 ± 10.4	-1068.0 ± 5.8
Q40TH315	2.441 ± 0.014	9.165 ± 0.068	2.464 ± 0.083	13.933 ± 0.039	120.6 ± 1.3	-39.4 ± 0.6	328.5 ± 2.9
Q50TH000	2.814 ± 0.013	4.089 ± 0.0848	7.762 ± 0.092	16.672 ± 0.023	-109.8 ± 3.1	159.5 ± 7.5	-77.3 ± 8.8
Q50TH090	2.865 ± 0.018	-8.094 ± 0.0421	4.566 ± 0.198	17.499 ± 0.336	623.4 ± 1.9	-75.4 ± 13.3	-1118.0 ± 7.8
Q50TH130	2.991 ± 0.017	-9.082 ± 0.1534	-2.150 ± 0.025	17.597 ± 0.114	688.2 ± 6.8	611.5 ± 20.9	-1330.0 ± 1.0
Q50TH210	2.805 ± 0.014	0.087 ± 0.0538	-8.922 ± 0.098	16.83 ± 0.089	9.5 ± 4.9	-221.3 ± 5.7	590.5 ± 9.9
Q50TH315	2.985 ± 0.018	8.788 ± 0.1391	2.945 ± 0.0222	17.43 ± 0.0177	600.4 ± 8.4	665.1 ± 20.4	1253.4 ± 2.4
Q66TH000	3.277 ± 0.012	3.404 ± 0.1164	7.633 ± 0.0533	20.177 ± 0.193	-69.7 ± 0.9	-294.6 ± 2.2	-848.5 ± 9.2
Q66TH090	3.419 ± 0.013	-8.028 ± 0.0443	3.166 ± 0.2086	21.293 ± 0.133	749.2 ± 6.2	17.3 ± 11.4	-1565.8 ± 11.9
Q66TH130	3.344 ± 0.012	-7.896 ± 0.1482	-2.756 ± 0.2232	20.736 ± 0.060	356.3 ± 1.0	425.9 ± 11.8	-940.4 ± 2.3
Q66TH210	3.336 ± 0.013	0.927 ± 0.1165	-8.427 ± 0.0148	20.701 ± 0.048	221.8 ± 7.5	-487.5 ± 2.9	1265.4 ± 11.0
Q66TH315	3.321 ± 0.011	7.628 ± 0.1358	3.368 ± 0.1800	20.651 ± 0.087	259.2 ± 3.6	404.5 ± 11.2	750.7 ± 3.2
Q100TH000	3.580 ± 0.006	2.036 ± 0.1025	6.224 ± 0.0869	23.232 ± 0.038	-10.2 ± 2.6	-447.0 ± 2.6	-1354.5 ± 5.2
Q100TH090	3.538 ± 0.004	-6.452 ± 0.2779	2.110 ± 0.2082	23.541 ± 0.332	344.2 ± 11.2	31.1 ± 3.3	-962.9 ± 4.6
Q100TH130	3.461 ± 0.001	-6.393 ± 0.3509	-2.042 ± 0.3155	22.749 ± 0.003	-46.7 ± 14.3	6.8 ± 3.8	245.1 ± 12.6
Q100TH210	3.606 ± 0.011	1.268 ± 0.0057	-6.940 ± 0.5645	23.382 ± 0.072	241.4 ± 0.6	-418.6 ± 0.3	1406.9 ± 2.8
Q100TH315	3.466 ± 0.001	6.268 ± 0.4289	2.608 ± 0.2515	22.748 ± 0.035	-77.6 ± 12.7	-34.8 ± 3.4	-383.3 ± 12.9
Q25TH000HR	1.605 ± 0.022	4.623 ± 0.025	5.699 ± 0.014	7.503 ± 0.124	110.2 ± 3.1	539.2 ± 0.2	471.9 ± 4.6
Q25TH090HR	1.632 ± 0.022	-6.164 ± 0.050	4.759 ± 0.049	7.668 ± 0.008	-698.5 ± 1.7	104.1 ± 6.2	504.7 ± 4.5
Q25TH130HR	1.736 ± 0.021	-7.811 ± 0.057	-0.682 ± 0.012	7.793 ± 0.012	-683.3 ± 2.4	-549.1 ± 13.4	400.6 ± 1.6
Q25TH210HR	1.629 ± 0.022	-1.129 ± 0.002	-7.430 ± 0.038	7.622 ± 0.134	-245.6 ± 8.2	656.9 ± 0.9	-512.7 ± 4.4
Q25TH315HR	1.715 ± 0.020	7.618 ± 0.043	1.323 ± 0.023	7.692 ± 0.005	-539.0 ± 1.7	-549.2 ± 11.6	-300.4 ± 0.7

TABLE III: The transformed spin (at $r = r_0$), recoil velocities in $\mathrm{km\,s^{-1}}$, and angles between the in-plane QXXXTH000 spins and the other QXXXTHYYY configurations in degrees. A '1' denotes a quantity measured using $(r_+, r_0, r_-)/M = (2.0, 1.0, 0.5)$, while a '2' denotes a quantity measured using $(r_+, r_0, r_-)/M = (2.2, 1.2, 0.7)$. The differences between the values given for $(2.0, 1.0, 0.5)$ and $(2.2, 1.2, 0.7)$ are indicative of the errors. Note that in the transformed system L_z and S_z are both negative (i.e. there is some partial spin/orbit alignment. We denote quantities in the (transformed) orbital plane with a $\perp$ subscript. The Q25THXXX quantities given on the bottom of the table are for the higher resolution runs. See Sec. III A for an explanation of the differences. The time derivative of the orbital separation $|\dot{r}|$ is a maximum at $r \sim 1.2$.

Config	$V_\perp(1)$	$V_\parallel(1)$	$a_\perp/m^H(1)$	$a_\parallel/m^H(1)$	$\vartheta(1)$	$V_\perp(2)$	$V_\parallel(2)$	$a_\perp/m^H(2)$	$a_\parallel/m^H(2)$	$\vartheta(2)$
Q13TH000	57.1362	-109.88	0.768518	-0.237098	0.	49.953	-113.327	0.751038	-0.291919	0.
Q13TH090	64.941	-97.8627	0.773066	-0.22036	3.63707	58.4083	-101.897	0.756446	-0.277112	3.96937
Q13TH130	220.34	-368.446	0.727118	-0.332954	-78.283	249.903	-349.071	0.761071	-0.249773	-77.2282
Q13TH210	42.1564	128.679	0.763202	-0.24517	177.413	31.9594	131.582	0.746572	-0.295965	177.276
Q13TH315	239.084	369.106	0.742796	-0.295281	87.2139	280.513	338.693	0.772431	-0.212227	89.2203
Q17TH000	309.622	568.413	0.751456	-0.270601	0.	370.742	530.574	0.776806	-0.193091	0.
Q17TH090	134.116	344.786	0.735493	-0.317919	67.034	123.344	348.784	0.738562	-0.314279	63.9956
Q17TH130	351.795	366.112	0.78253	-0.15129	-36.082	393.985	320.27	0.786039	-0.145002	-35.7209
Q17TH210	300.137	-563.416	0.746093	-0.279011	-176.311	357.269	-529.036	0.773073	-0.199299	-176.459
Q17TH315	283.	-156.073	0.784854	-0.145801	123.407	295.546	-130.769	0.778357	-0.186578	123.21
Q25TH000	373.905	-948.305	0.757314	-0.240225	0.	459.51	-909.911	0.77861	-0.167965	0.
Q25TH090	452.721	-870.357	0.779284	-0.154404	-21.2857	544.717	-815.942	0.788089	-0.114385	-21.0555
Q25TH130	197.85	48.3342	0.770647	-0.202858	-84.2701	195.719	56.3483	0.759915	-0.247894	-85.4253
Q25TH210	426.136	916.571	0.77451	-0.184646	165.452	521.338	865.968	0.787368	-0.131325	165.72
Q25TH315	124.649	-204.556	0.759673	-0.241429	85.9471	115.438	-209.892	0.750901	-0.274232	84.2327
Q33TH000	477.923	-1193.82	0.787385	-0.136406	0.	585.012	-1145.16	0.794072	-0.101676	0.
Q33TH090	506.036	-874.874	0.794658	-0.0857209	-23.2403	573.118	-832.474	0.794033	-0.100666	-23.2941
Q33TH130	121.993	393.11	0.754769	-0.264995	-83.3346	106.146	397.682	0.753714	-0.275061	-85.3148
Q33TH210	510.834	1029.22	0.793461	-0.100511	165.757	597.049	981.726	0.795102	-0.0964032	165.86
Q33TH315	142.073	-607.563	0.74435	-0.292739	85.1084	124.37	-611.433	0.751109	-0.280681	82.8364
Q40TH000	395.545	-1447.96	0.782576	-0.177756	0.	501.737	-1414.67	0.792558	-0.121423	0.
Q40TH090	506.998	-1223.4	0.797605	-0.0811617	-29.708	599.942	-1180.61	0.798469	-0.074772	-29.6255
Q40TH130	199.308	85.9742	0.773172	-0.20708	-88.1121	196.752	91.6738	0.767006	-0.237119	-89.0041
Q40TH210	468.966	1380.9	0.794067	-0.117055	163.468	578.675	1338.63	0.797642	-0.0855529	163.572
Q40TH315	138.257	-323.823	0.762353	-0.243806	82.1551	127.284	-328.291	0.760328	-0.257681	80.7494
Q50TH000	206.386	29.5953	0.775871	-0.197482	0.	205.713	33.9596	0.771006	-0.223791	0.
Q50TH090	211.758	1264.66	0.760737	-0.256772	-53.0652	228.683	1261.71	0.77738	-0.20449	-53.2402
Q50TH130	426.349	1560.33	0.793283	-0.105245	-109.529	530.071	1528.21	0.800072	-0.0682939	-108.518
Q50TH210	117.707	-619.58	0.759212	-0.259	158.194	100.605	-622.586	0.763761	-0.251091	157.494
Q50TH315	454.34	-1472.23	0.799245	-0.0784754	62.2872	549.566	-1439.4	0.799962	-0.065415	63.1927
Q66TH000	118.274	893.123	0.763607	-0.251388	0.	101.713	895.16	0.772394	-0.226846	0.
Q66TH090	268.896	1714.94	0.7931	-0.116783	-62.1364	354.418	1699.33	0.802482	-0.066631	-60.9979
Q66TH130	336.909	1038.86	0.80055	-0.0605261	-111.577	377.096	1024.96	0.797946	-0.0868091	-110.371
Q66TH210	163.971	-1364.27	0.770063	-0.232589	157.52	176.949	-1362.65	0.783732	-0.184392	157.808
Q66TH315	311.388	-835.099	0.798347	-0.0778683	60.8859	339.961	-823.881	0.795121	-0.109404	62.06
Q100TH000	88.5695	1423.66	0.79471	-0.158448	0.	108.207	1422.3	0.800356	-0.116206	0.
Q100TH090	134.476	1014.12	0.806191	-0.0286805	-65.6896	167.057	1009.26	0.803238	-0.0439484	-65.4866
Q100TH130	52.4647	-244.074	0.785337	-0.163234	-116.365	42.6164	-245.985	0.785246	-0.170854	-116.398
Q100TH210	95.9383	-1484.52	0.805662	-0.0736974	151.702	151.312	-1479.91	0.804525	-0.0475139	151.917
Q100TH315	55.0809	388.766	0.78288	-0.178353	58.0786	40.6688	390.537	0.78611	-0.178897	57.8702
Q25TH000HR	238.923	-684.464	0.727703	-0.328834	0	235.693	-685.583	0.744828	-0.292768	0
Q25TH090HR	302.537	-813.638	0.731821	-0.318884	-12.0909	317.701	-807.838	0.754461	-0.263398	-11.4989
Q25TH130HR	514.081	-815.226	0.787921	-0.127218	-83.1554	596.917	-756.679	0.791774	-0.114032	-80.3582
Q25TH210HR	299.288	815.542	0.730048	-0.325618	167.319	315.17	809.537	0.753828	-0.269311	167.829
Q25TH315HR	501.346	656.57	0.79009	-0.113807	85.1511	560.613	606.749	0.789798	-0.127652	87.8788

FIG. 5: A fit of $v_{\parallel}$ for the $q = 1, 2/3, 1/2, 1/2.5, 1/3, 1/4, 1/6, 1/8$, and the high-resolution $q = 1/4$ runs (from top to bottom) with the plane chosen by the points on the trajectory with $(r_+, r_0, r_-) = (2, 1, 0.5)$ (left) and $(r_+, r_0, r_-) = (2.2, 1.2, 0.7)$ (right).

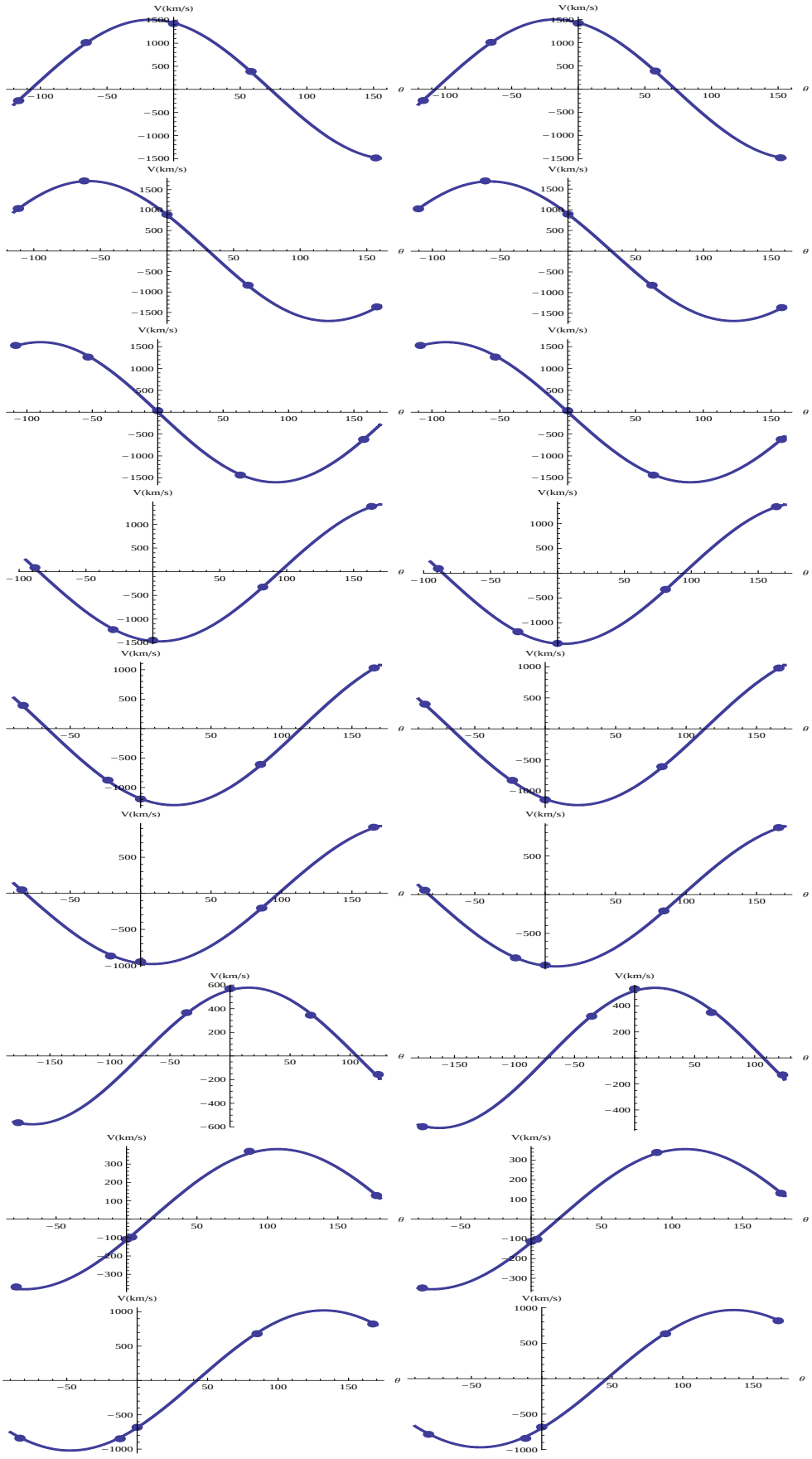

TABLE IV: Fit parameters for $v_\parallel = A\cos((\vartheta - B)\pi/180)$ for each q. A is in units of $\mathrm{km\,s^{-1}}$ and B is in degrees. A (1) denotes values obtained from the $(r_+, r_0, r_-) = (2, 1, 0.5)$ transformation, while a (2) denotes values obtained from the $(r_+, r_0, r_-) = (2.2, 1.2, 0.7)$ transformation. The last row shows A and B when the grid is refined by a factor of 1.2

q	A(1)	B(1)	A(2)	B(2)
1/8	381.2 ± 7.1	107.33 ± 0.93	355.7 ± 4.4	109.35 ± 0.63
1/6	577 ± 11	15.51 ± 1.18	538 ± 12	17.2 ± 1.4
1/4	981 ± 11	188.03 ± 0.70	926.3 ± 5.1	187.61 ± 0.33
1/3	1297.8 ± 9.2	203.75 ± 0.37	1231.7 ± 9.5	203.22 ± 0.41
1/2.5	1472.4 ± 9.6	184.88 ± 0.39	1424.1 ± 5.1	184.35 ± 0.21
1/2	1640 ± 23	269.96 ± 0.77	1603 ± 15	270.32 ± 0.54
2/3	1709.1 ± 7.7	301.26 ± 0.26	1686.0 ± 8.6	246.04 ± 0.30
1	1508.1 ± 8.7	342.69 ± 0.32	1502.5 ± 6.7	342.76 ± 0.25
1/4	994.6 ± 6.4	133.03 ± 0.43	942.5 ± 4.6	137.09 ± 0.35

at $q = 2/3$. Baker et al. [57] propose that Eq. (1) should be modified to $v_\parallel = 4K\eta^3/(1+q)(\alpha_1 - q\alpha_2)$ (which has a maximum at $q = 3/4$ for fixed α_1 and $\alpha_2 = 0$). In order to discriminate between these two possibilities we fit our data to the form

$$v_\parallel/\alpha = G(4\eta)^H/(16(1+q)), \tag{9}$$

where we set $G = K$ and solve for H, as well as allowing both G and H to vary. Here $\alpha = |\alpha_1^\perp - q\alpha_2^\perp|$. It is important to note that our fits use eight values of q to obtain one or two parameters. In Figs. 6, 7, and 8 we show results from these fits for the choices $(r_+, r_0, r_-) = (2, 1, 0.5)$ and $(r_+, r_0, r_-) = (2.2, 1.2, 0.7)$. In the figures we plot the predicted recoil velocity using both our formula and the one proposed by Baker et al. assuming an uncertainty in K twice as large as that given in [3]. From the plots we can see that the recoil velocities agree with our empirical formula much better than with the Baker et al. modification. The best fit functions have the form $v_\parallel/\alpha = K\eta^{1.91\pm0.062}/(1+q)$ (with a root mean square error in the predicted v/α of $68\ \mathrm{km\,s^{-1}}$) and $v_\parallel/\alpha = K\eta^{2.036\pm0.046}/(1+q)$ (with a root mean square error in v/α of $46\ \mathrm{km\,s^{-1}}$) for the choices $(r_+, r_0, r_-) = (2, 1, 0.5)$ and $(r_+, r_0, r_-) = (2.2, 1.2, 0.7)$ respectively, where K was set to $K = 6.0 \times 10^4$, and $v_\parallel/\alpha = (62965 \pm 746)\eta^{2.027\pm0.048}/(1+q)$ (with a root mean square error in the predicted v/α of $35\ \mathrm{km\,s^{-1}}$) and $v_\parallel/\alpha = (62024 \pm 555)\eta^{2.127\pm0.037}/(1+q)$ (with a root mean square error in the predicted v/α of $26\ \mathrm{km\,s^{-1}}$) respectively when both G and H are varied. The value of the constant $K = G_{\rm fit}$ determined in these latter two fits is in reasonable agreement with our previous measurement of $K = (6.0 \pm 0.1) \times 10^4$.

A. Finite difference errors

The effect of finite difference errors are most significant for the smaller q runs. Here the main effect regarding our calculation is that the ϑ is rotated with respect to its analytic value (See e.g. [54]). This means that, although there may be significant errors in both the magnitude and direction of the recoil in a particular run, the maximum recoil (as determined by the fit (8)) for a given q is relatively insensitive to this error. This can be seen in the dependence of A in Eq. (8) on resolution for the $q = 1/4$ case in Table IV. This relatively small difference is smaller than the mean error in the fits to the form (9). If we perform the fit to form (9) using the high-resolution $q = 1/4$ results, then the fitting parameters change from $(G = 62965 \pm 746, H = 2.03 \pm 0.04)$ to $(G = 62908 \pm 805, H = 2.01 \pm 0.05)$ and from $(G = 62023 \pm 555, H = 2.13 \pm .04)$ to $(G = 61974 \pm 584, H =$

FIG. 6: Fit of out-of-plane recoil $(V_\parallel/\alpha)$ versus mass ratio q for the $(r_+, r_0, r_-) = (2, 1, 0.5)$ choice of orbital plane. The top shaded region shows our predicted value for $K = (6.0 \pm 0.2) \times 10^4$, the lower region shows the prediction based on the modification proposed by Baker et al., the green curve shows a fit to η^n, while the blue curve has a simultaneous fit to η^n and K. Note that the measured values of $V_\parallel/\alpha$, while slightly overshooting the predictions, agree much better with our $\mathcal{O}(\eta^2)$ form.

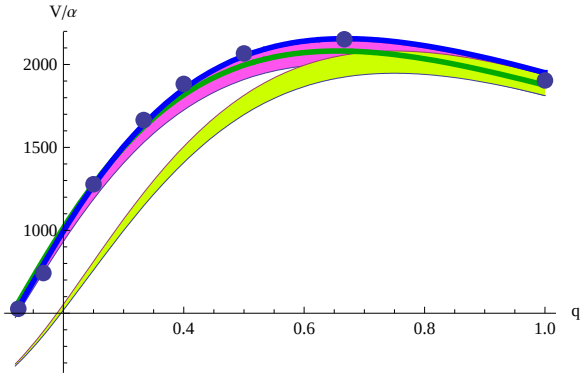

FIG. 7: Fit of out-of-plane recoil $(V_\parallel/\alpha)$ versus mass ratio q for the $(r_+, r_0, r_-) = (2.2, 1.2, 0.7)$ choice of orbital plane. The top shaded region shows our predicted value for $K = (6.0 \pm 0.2) \times 10^4$, the lower region shows the prediction based on the modification proposed by Baker et al., the green curve shows a fit to η^n, while the blue curve has a simultaneous fit to η^n and K. Here we see very good agreement between the measured $V_\parallel/\alpha$ and our prediction.

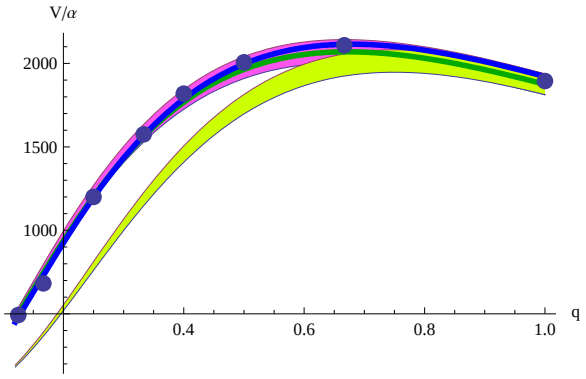

FIG. 8: The out-of-plane recoil ($V_\parallel/\alpha$) versus mass ratio q for both choices of (r_+, r_0, r_-) as well as the predictions assuming a leading η^2 and η^3 dependence. The solid lines show the prediction assuming a leading η^2 dependence and an error in K of 0.2×10^4 km s^{-1}, while the dotted lines show the prediction assuming a leading η^3 dependence and an error in K of 0.2×10^4 km s^{-1}. The $((r_+, r_0, r_-) = (2, 1, 0.5)$ data points lie above the $(2.2, 1.2.0.7)$ data points. The $(2.2, 1.2.0.7)$ data points lie closer to the predicted values, which is consistent with the observation that $r_0 = 1.2$ is a better approximation to the location of the maximum of $|\dot{r}|$ for all configurations than $|\dot{r} = 1|$. The differences in these data points (for a given q) is indicative of the true error in calculating the out-of-plane recoil.

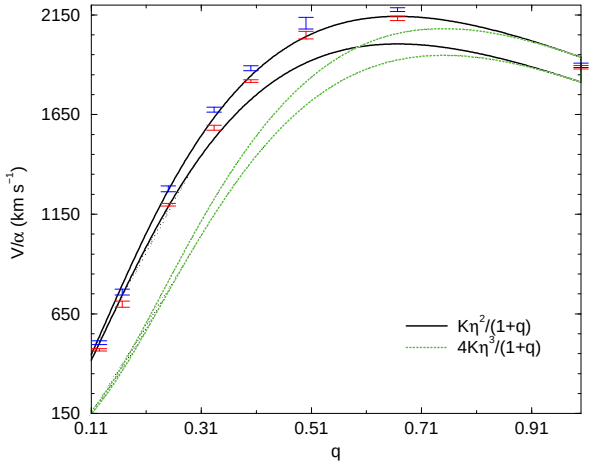

2.11 ± 0.04) for the choices $(r_+, r_0, r_-) = (2, 1, 0.5)$ and $(r_+, r_0, r_-) = (2.2, 1.2, 0.7)$ respectively (i.e. the change is not statistically significant).

Note that although we expect the $q = 1/6$ and $q = 1/8$ results to be less accurate than those of the more modest mass ratio cases, including these simulations does not change the observed η dependence. This strongly suggests that the η dependence is robust against finite difference errors.

We note that very recent work in PN prediction of the recoil [74] and perturbative calculations (a work in progress by the authors) show that there is an η^3 correction to the leading η^2 dependence of the out-of-plane recoil. An attempt to fit our data to the functional form $V/\alpha = (A\eta^2 + B\eta^3)/(1 + q)$ does not yield an accurate evaluation of B because the functional form of the recoil is insensitive to B at the level of accuracy we obtained. That is to say, even if B is large, for example $B \sim 39000$ and $A \sim 52000$ is correspondingly smaller (such that $B\eta^3 + A\eta^2 \sim 60000/16$ when $\eta = 1/4$) the maximum change in the predicted recoil is of order 10 km s^{-1} over the entire range of η. We note that both the PN and perturbative predictions include a leading order η^2 dependence for all configurations including those of Baker et al. [57].

B. The In-Plane Kick

Examining Table III, we see that the magnitude of the in-plane recoil $v_\perp$ is far larger than that predicted by Eq. (1) (the maximum predicted in-plane recoil velocity for the unequal mass cases is about 100 - 200 km s^{-1} and is dominated by the unequal-mass, rather than spin, component of the recoil; while for the equal-mass case, the in-plane recoil is ~ 50 km s^{-1}), and that the difference in the magnitude for two choices of (r_+, r_0, r_-) are significant (around 25%). One possibility is simply that the direction of the orbital angular momentum was not measured with sufficient accuracy. If this is the case, then since the out-of-plane recoil is of order 1000 km s^{-1}, an error in the determination direction of the orbital angular momentum direction of 20°, would lead to an error in the in-plane recoil of 350 km s^{-1} (or 200%), but an error in the out-of-plane recoil of only 60 km s^{-1} (or 6%). Thus this seems to be a plausible explanation. However, as seen in Fig. 6 we appear to overestimate the out-of-plane recoil to a moderate degree. Another possible explanation is that the recoil due to unequal masses is a function of the acceleration of the masses, and is thus a function of the trajectories. Our trajectories differ significantly from the non-spinning, unequal mass trajectories. Thus Eq. (2a) may underestimate the unequal-mass component of the recoil in these cases. Finally we note that the unequal-mass component of the recoil is small due to cancellations in the radiated linear momentum between each half of the orbit. That is, the more symmetric the orbit, the less net linear momentum radiated. Since our orbits precess, there is likely less cancellation.

C. An alternative choice for the plane

In this section we reanalyze the recoil velocities using a choice of orbital plane adapted to each individual run. In Fig. 9 we show $\ddot{r}(t)$ as a function of r during the merger. From the figure we can see that there is some scatter in the locations of the zero, maximum, and minimum of $\ddot{r}(t)$, but are generally independent of both the initial angle and mass ratio (this observation justifies our choice above of using fixed choices for (r_+, r_0, r_-)). In this analysis we chose r_+ to be the location of the minimum in $\ddot{r}(t)$, r_0 to be the location of the zero (i.e. location where $|\dot{r}(t)|$ is maximized), and r_- to be the location of the maximum in $\ddot{r}(t)$. This choice has the advantage that we do not use any 'fiducial' choices for (r_+, r_0, r_-). Table V summarizes the results for the transformed recoil velocities and kicks, while Table VI summarizes the fit parameters A and B after fitting the results from each mass ratio to the form (8). A fit of the maximum recoil velocity per mass ratio to the form (9) yields $H = 1.904 \pm 0.041$ when $G = K$ and ($H = 1.954 \pm 0.05$, $G = (6151 \pm 804)$km s^{-1}) when both H and G are allowed to vary. These results are in good agreement with those for the fixed choices of (r_+, r_0, r_-). Finally, in Fig. 10

FIG. 9: Md^2r/dt^2 versus r/M as a function of mass ratio and initial spin orientation. Note that the locations of the zero, minima, and a maxima are very similar.

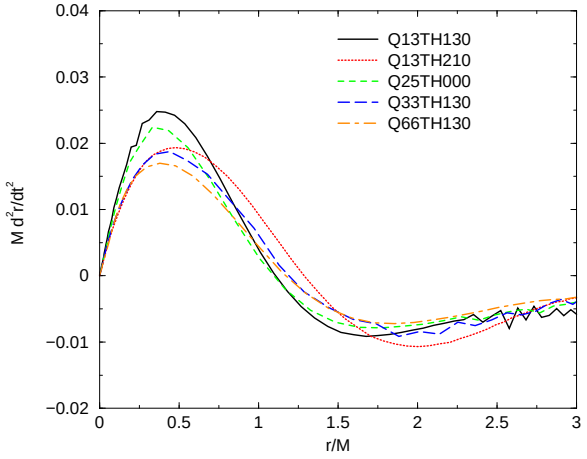

FIG. 10: The out-of-plane recoil ($V_\parallel/\alpha$) versus mass ratio q for the adaptive choice of (r_+, r_0, r_-) as well as the predictions assuming a leading η^2 and η^3 dependence. The solid lines show the prediction assuming a leading η^2 dependence and an error in K of 0.2×10^4 km s^{-1}, while the dotted lines show the prediction assuming a leading η^3 dependence and an error in K of 0.2×10^4 km s^{-1}.

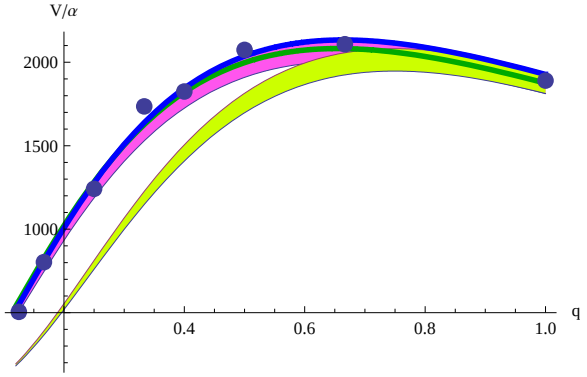

we show fits of the maximum out-of-plane recoil versus mass ratio using this choice of adaptive plane parameters. Note that with this method the scatter in the plot is more significant, indicating that a fixed choice of plane parameters produces a more robust estimate of the out-of-plane recoil. We also note that the choice of plane parameters $(r_+, r_0, r_0) = (2.2, 1.2, 0.7)$ gives the best fits, which is consistent with the observation that $r_0 = 1.2$ is well adapted to the locations of the maximum in $|\dot{r}|$ for the runs considered here.

Finally, we note that the error in the recoil velocities due to finite starting time were of order 10 km s^{-1} in each direction for all runs. We estimated these errors by looking for a systematic offset in the recoil velocity when plotted as a function of time (See Fig 11). These errors, while not insignificant do not change the results of our analysis because they are the same order as the errors

TABLE V: The transformed spin (at $r = r_0$), recoil velocities in km s^{-1}, and angles between the in-plane QXXXTH000 spins and the other QXXXTHYYY configurations in degrees when r_+ is chosen to be the value of r when $\ddot{r}(t)$ reaches its minimum, r_0 is the value of r when $\ddot{r}(t) = 0$ (i.e. when $|\dot{r}(t)|$ is at its maximum), and r_- is the value of r when $\ddot{r}(t)$ reaches its maximum. Note that in the transformed system L_z and S_z are both negative (i.e. there is some partial spin/orbit alignment. We denote quantities in the (transformed) orbital plane with a $\perp$ subscript.

Config	$V_\perp$	$V_\parallel$	$a_\perp/m^H$	$a_\parallel/m^H$	ϑ
Q13TH000	52.1681	-112.324	0.770573	-0.236828	0.
Q13TH090	58.7557	-101.697	0.7674	-0.246703	1.29153
Q13TH130	213.996	-372.167	0.715948	-0.357787	-55.7042
Q13TH210	37.8511	130.01	0.764949	-0.244748	-178.98
Q13TH315	234.147	372.257	0.733002	-0.319972	105.641
Q17TH000	278.533	584.276	0.73713	-0.307434	0.
Q17TH090	133.506	345.022	0.747727	-0.292225	56.9267
Q17TH130	405.804	305.157	0.796759	-0.0790985	-66.0061
Q17TH210	273.036	-577.037	0.729478	-0.32118	-170.825
Q17TH315	303.864	-110.066	0.797954	-0.0710164	87.869
Q25TH000	328.136	-965.098	0.74441	-0.277851	0.
Q25TH090	368.549	-909.203	0.767864	-0.203131	-20.4251
Q25TH130	194.765	59.5598	0.777913	-0.186817	-111.668
Q25TH210	340.595	951.677	0.758298	-0.24157	167.113
Q25TH315	122.309	-205.964	0.771452	-0.210448	73.1503
Q33TH000	432.797	-1210.91	0.784273	-0.156319	0.
Q33TH090	522.116	-865.374	0.797412	-0.0611074	-36.3755
Q33TH130	123.321	392.695	0.764043	-0.242325	-87.9496
Q33TH210	538.156	1015.2	0.798003	-0.0555484	148.237
Q33TH315	160.341	-603.	0.755614	-0.263486	78.0326
Q40TH000	345.769	-1460.64	0.777363	-0.199695	0.
Q40TH090	464.445	-1240.18	0.795298	-0.0996155	-31.0583
Q40TH130	199.788	84.8549	0.779402	-0.184948	-97.0931
Q40TH210	358.115	1413.71	0.783135	-0.174788	177.471
Q40TH315	138.301	-323.804	0.77561	-0.207095	73.4494
Q50TH000	206.224	30.7051	0.780222	-0.185459	0.
Q50TH090	216.108	1263.93	0.77053	-0.230075	-47.8033
Q50TH130	351.439	1578.89	0.789517	-0.13106	-98.1525
Q50TH210	122.003	-618.748	0.768792	-0.235123	158.316
Q50TH315	379.77	-1493.21	0.797621	-0.0947157	68.7318
Q66TH000	134.205	890.868	0.769565	-0.233273	0.
Q66TH090	253.359	1717.31	0.797964	-0.106154	-50.8354
Q66TH130	324.629	1042.76	0.800428	-0.0583467	-100.477
Q66TH210	164.115	-1364.25	0.769748	-0.233049	171.955
Q66TH315	296.905	-840.357	0.799556	-0.0682437	72.8232
Q100TH000	89.5687	1423.6	0.793956	-0.16161	0.
Q100TH090	119.496	1015.99	0.804421	-0.0421833	-66.5996
Q100TH130	52.4861	-244.07	0.789395	-0.14723	-119.948
Q100TH210	80.6623	-1485.43	0.803926	-0.0816034	151.372
Q100TH315	60.4502	387.967	0.788101	-0.157316	56.6673

FIG. 11: The recoil velocity versus time for various mass ratios for the $\Theta = 0$ configurations (top left: $q = 1/8$, top right: $q = 1/4$, bottom left: $q = 2/3$, bottom right: $q = 1$). The error in the recoil due to not including the correct initial value has the effect of translating the plots. This error appears to be no more than $\sim 10\ \mathrm{km\,s^{-1}}$.

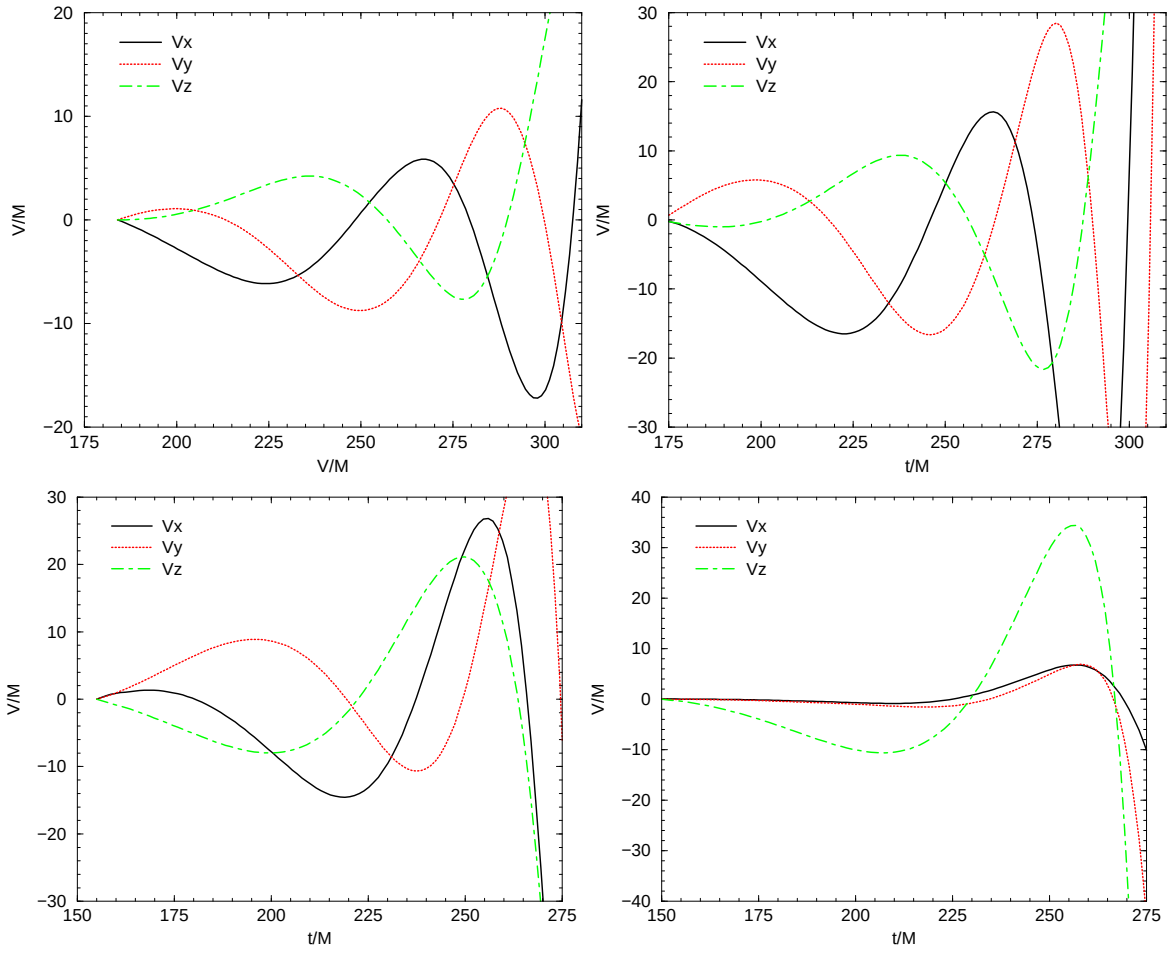

TABLE VI: Fit parameters for $v_{\parallel} = A\cos((\vartheta - B)\pi/180)$ for each q. A is in units of $\mathrm{km\,s^{-1}}$ and B is in degrees for the adapted choice of plane parameters (r_+, r_0, r_-).

q	A	B
1/8	379.0 ± 9.9	108.51 ± 1.33
1/6	611.4 ± 37.4	353.47 ± 3.33
1/4	948.5 ± 55.6	169.16 ± 4.08
1/3	1353.4 ± 66.5	195.32 ± 2.34
1/2.5	1427.5 ± 15.6	176.70 ± 0.72
1/2	1620.5 ± 16.7	271.46 ± 0.60
2/3	1659.9 ± 82.8	310.17 ± 3.05
1	1504.9 ± 15.3	340.60 ± 0.56

due to extrapolations to infinity and the errors in the fits of the recoil.

IV. CONCLUSION

In this paper we explored the merger recoil from precessing black-hole binaries with a larger spinning black hole (with initial spin $a/m = 0.8$) in quasi-circular orbit with a smaller non-spinning black hole. We introduced techniques to determine the normal to the orbital plane at merger and thus decompose the recoil into its in-plane

and out-of plane components. However, there are important open questions about the accuracy of the determination of the orbital plane, the spin direction, and spin magnitude. All these quantities are measured in the highly dynamical region around the merger. In this work we have introduced techniques to begin studying this problem that will need to be refined. The issue of the in-plane recoil is particularly important, because large in-plane recoils imply that our heuristic formula needs to be modified for strongly precessing binaries. Nevertheless, our results, as seen in Fig. 8, indicate that the out-of-plane recoil has an $\mathcal{O}(\eta^2)$ rather than $\mathcal{O}(\eta^3)$ leading-order dependence on the symmetric mass ratio. This result, while agreeing with our prediction, appears to disagree with the recent work of Baker et al. [57]. Thus additional work with new configurations may be needed in order to determine leading-order dependence, or indeed, if this dependence is a function of the configuration.

Acknowledgments

We thank Manuela Campanelli for many valuable discussions. We gratefully acknowledge NSF for financial support from grant PHY-0722315, PHY-0653303, PHY 0714388, and PHY 0722703; and NASA for financial support from grant NASA 07-ATFP07-0158. Computational resources were provided by Lonestar cluster at TACC and by NewHorizons at RIT.

[1] S. Komossa, H. Zhou, and H. Lu, Astrop. J. Letters **678**, L81 (2008), 0804.4585.
[2] M. Campanelli, C. O. Lousto, Y. Zlochower, and D. Merritt, Astrophys. J. **659**, L5 (2007), gr-qc/0701164.
[3] M. Campanelli, C. O. Lousto, Y. Zlochower, and D. Merritt, Phys. Rev. Lett. **98**, 231102 (2007), gr-qc/0702133.
[4] T. Bogdanovic, C. S. Reynolds, and M. C. Miller (2007), astro-ph/0703054.
[5] A. Loeb, Phys. Rev. Lett. **99**, 041103 (2007), astro-ph/0703722.
[6] E. W. Bonning, G. A. Shields, and S. Salviander (2007), 0705.4263.
[7] K. Holley-Bockelmann, K. Gultekin, D. Shoemaker, and N. Yunes (2007), 0707.1334.
[8] S. Komossa and D. Merritt, Astrophys. J. **683**, L21 (2008), 0807.0223.
[9] F. Pretorius, Phys. Rev. Lett. **95**, 121101 (2005), gr-qc/0507014.
[10] M. Campanelli, C. O. Lousto, P. Marronetti, and Y. Zlochower, Phys. Rev. Lett. **96**, 111101 (2006), gr-qc/0511048.
[11] J. G. Baker, J. Centrella, D.-I. Choi, M. Koppitz, and J. van Meter, Phys. Rev. Lett. **96**, 111102 (2006), gr-qc/0511103.
[12] M. Campanelli, C. O. Lousto, and Y. Zlochower, Phys. Rev. D **73**, 061501(R) (2006).
[13] J. G. Baker, J. Centrella, D.-I. Choi, M. Koppitz, and J. van Meter, Phys. Rev. D **73**, 104002 (2006), gr-qc/0602026.
[14] M. Campanelli, C. O. Lousto, and Y. Zlochower, Phys. Rev. D **74**, 041501(R) (2006), gr-qc/0604012.
[15] M. Campanelli, C. O. Lousto, and Y. Zlochower, Phys. Rev. D **74**, 084023 (2006), astro-ph/0608275.
[16] M. Campanelli, C. O. Lousto, Y. Zlochower, B. Krishnan, and D. Merritt, Phys. Rev. **D75**, 064030 (2007), gr-qc/0612076.
[17] F. Pretorius, Class. Quant. Grav. **23**, S529 (2006), gr-qc/0602115.
[18] F. Pretorius and D. Khurana, Class. Quant. Grav. **24**, S83 (2007), gr-qc/0702084.
[19] J. G. Baker, J. R. van Meter, S. T. McWilliams, J. Centrella, and B. J. Kelly, Phys. Rev. Lett. **99**, 181101 (2007), gr-qc/0612024.
[20] B. Brugmann et al., Phys. Rev. **D77**, 024027 (2008), gr-qc/0610128.
[21] A. Buonanno, G. B. Cook, and F. Pretorius, Phys. Rev. **D75**, 124018 (2007), gr-qc/0610122.
[22] J. G. Baker et al., Phys. Rev. **D75**, 124024 (2007), gr-qc/0612117.
[23] M. A. Scheel et al., Phys. Rev. **D74**, 104006 (2006), gr-qc/0607056.
[24] J. G. Baker, M. Campanelli, F. Pretorius, and Y. Zlochower, Class. Quant. Grav. **24**, S25 (2007), gr-qc/0701016.
[25] P. Marronetti et al., Class. Quant. Grav. **24**, S43 (2007), gr-qc/0701123.
[26] H. P. Pfeiffer et al., Class. Quant. Grav. **24**, S59 (2007), gr-qc/0702106.
[27] M. Campanelli, Class. Quant. Grav. **22**, S387 (2005), astro-ph/0411744.
[28] F. Herrmann, D. Shoemaker, and P. Laguna, AIP Conf. **873**, 89 (2006), gr-qc/0601026.
[29] J. G. Baker et al., Astrophys. J. **653**, L93 (2006), astro-ph/0603204.
[30] C. F. Sopuerta, N. Yunes, and P. Laguna, Phys. Rev. D **74**, 124010 (2006), astro-ph/0608600.
[31] J. A. González, U. Sperhake, B. Brugmann, M. Hannam, and S. Husa, Phys. Rev. Lett. **98**, 091101 (2007), gr-qc/0610154.
[32] C. F. Sopuerta, N. Yunes, and P. Laguna, Astrophys. J. **656**, L9 (2007), astro-ph/0611110.
[33] F. Herrmann, I. Hinder, D. Shoemaker, and P. Laguna, AIP Conf. Proc. **873**, 89 (2006).
[34] F. Herrmann, I. Hinder, D. Shoemaker, and P. Laguna, Class. Quant. Grav. **24**, S33 (2007).
[35] F. Herrmann, I. Hinder, D. Shoemaker, P. Laguna, and R. A. Matzner, Astrophys. J. **661**, 430 (2007), gr-qc/0701143.
[36] M. Koppitz et al., Phys. Rev. Lett. **99**, 041102 (2007), gr-qc/0701163.
[37] D.-I. Choi et al., Phys. Rev. **D76**, 104026 (2007), gr-qc/0702016.
[38] J. A. González, M. D. Hannam, U. Sperhake, B. Brugmann, and S. Husa, Phys. Rev. Lett. **98**, 231101 (2007), gr-qc/0702052.
[39] J. G. Baker et al., Astrophys. J. **668**, 1140 (2007), astro-

ph/0702390.
[40] E. Berti et al., Phys. Rev. **D76**, 064034 (2007), gr-qc/0703053.
[41] W. Tichy and P. Marronetti, Phys. Rev. **D76**, 061502 (2007), gr-qc/0703075.
[42] F. Herrmann, I. Hinder, D. M. Shoemaker, P. Laguna, and R. A. Matzner, Phys. Rev. **D76**, 084032 (2007), 0706.2541.
[43] B. Brugmann, J. A. Gonzalez, M. Hannam, S. Husa, and U. Sperhake, Phys. Rev. **D77**, 124047 (2008), 0707.0135.
[44] J. D. Schnittman et al., Phys. Rev. **D77**, 044031 (2008), 0707.0301.
[45] B. Krishnan, C. O. Lousto, and Y. Zlochower, Phys. Rev. **D76**, 081501 (2007), 0707.0876.
[46] D. Pollney et al., Phys. Rev. **D76**, 124002 (2007), 0707.2559.
[47] S. Dain, C. O. Lousto, and Y. Zlochower, Phys. Rev. D **78**, 024039 (2008), 0803.0351.
[48] I. H. Redmount and M. J. Rees, Comments on Astrophysics **14**, 165 (1989).
[49] D. Merritt, M. Milosavljevic, M. Favata, S. A. Hughes, and D. E. Holz, Astrophys. J. **607**, L9 (2004), astro-ph/0402057.
[50] A. Gualandris and D. Merritt (2007), 0708.0771.
[51] R. C. Kapoor, Pramana **7**, 334 (1976).
[52] M. J. Fitchett, MNRAS **203**, 1049 (1983).
[53] L. E. Kidder, Phys. Rev. D **52**, 821 (1995), gr-qc/9506022.
[54] C. O. Lousto and Y. Zlochower, Phys. Rev. **D77**, 044028 (2008), 0708.4048.
[55] L. Boyle, M. Kesden, and S. Nissanke, Phys. Rev. Lett. **100**, 151101 (2008), 0709.0299.
[56] L. Boyle and M. Kesden (2007), 0712.2819.
[57] J. G. Baker et al., Astrophys. J. **682**, L29 (2008), 0802.0416.
[58] S. Brandt and B. Brügmann, Phys. Rev. Lett. **78**, 3606 (1997), gr-qc/9703066.
[59] M. Ansorg, B. Brügmann, and W. Tichy, Phys. Rev. D **70**, 064011 (2004), gr-qc/0404056.
[60] Y. Zlochower, J. G. Baker, M. Campanelli, and C. O. Lousto, Phys. Rev. D **72**, 024021 (2005), gr-qc/0505055.
[61] T. Nakamura, K. Oohara, and Y. Kojima, Prog. Theor. Phys. Suppl. **90**, 1 (1987).
[62] M. Shibata and T. Nakamura, Phys. Rev. D **52**, 5428 (1995).
[63] T. W. Baumgarte and S. L. Shapiro, Phys. Rev. D **59**, 024007 (1999), gr-qc/9810065.
[64] P. Marronetti, W. Tichy, B. Brugmann, J. Gonzalez, and U. Sperhake, Phys. Rev. **D77**, 064010 (2008), 0709.2160.
[65] C. O. Lousto and Y. Zlochower, Phys. Rev. **D77**, 024034 (2008), 0711.1165.
[66] Cactus Computational Toolkit home page: `http://www.cactuscode.org`.
[67] E. Schnetter, S. H. Hawley, and I. Hawke, Class. Quantum Grav. **21**, 1465 (2004), gr-qc/0310042.
[68] M. Alcubierre, B. Brügmann, P. Diener, M. Koppitz, D. Pollney, E. Seidel, and R. Takahashi, Phys. Rev. D **67**, 084023 (2003), gr-qc/0206072.
[69] C. Gundlach and J. M. Martin-Garcia, Phys. Rev. **D74**, 024016 (2006), gr-qc/0604035.
[70] J. Thornburg, Class. Quantum Grav. **21**, 743 (2004), gr-qc/0306056.
[71] O. Dreyer, B. Krishnan, D. Shoemaker, and E. Schnetter, Phys. Rev. D **67**, 024018 (2003), gr-qc/0206008.
[72] M. Campanelli and C. O. Lousto, Phys. Rev. D **59**, 124022 (1999), gr-qc/9811019.
[73] C. O. Lousto and Y. Zlochower, Phys. Rev. D **76**, 041502(R) (2007), gr-qc/0703061.
[74] E. Racine, A. Buonanno, and L. E. Kidder (2008), 0812.4413.